



Numerical study of coupled electromagnetic and aerothermodynamic phenomena in a circuit breaker electric arc

Hélène Rachard^{a,*}, Pierre Chévrier^a, Daniel Henry^b, Denis Jeandel^b

^a Centre de recherche Schneider Electric, 38000 Grenoble, France

^b Laboratoire de Mécanique des Fluides et d'Acoustique—UMR CNRS 5509 Ecole Centrale de Lyon/Université Claude Bernard—Lyon 1 ECL, BP163, 69131 Ecully Cedex, France

Received 26 May 1997; in final form 18 January 1998

Abstract

Two-dimensional simulations of electric arcs in air in a low-voltage circuit breaker have been performed. For this purpose, a compressible hydrodynamic code taking into account the properties of the arc plasma and the electric, magnetic and radiative phenomena has been developed. A whole evolution of the arc from its ignition to its stagnation at the end of the chamber after displacement has been simulated. The analysis of the results shows the flow compression by the pressure waves and the influence of the magnetic forces on the shape and displacement of the arc. It has been established that the viscosity has little influence on the evolution. © 1998 Elsevier Science Ltd. All rights reserved.

Nomenclature

B magnetic induction
 c speed of sound
 e internal density energy
 E total energy
 E_{arc} electrical field
 F Laplace force
 h length of arc column
 i current
 j current density flux
 p pressure
 q flux of conduction
 r_0 perfect gas constant
 R_{arc} arc resistance
 R_{ay} net emission of radiation
 S_a arc section
 T temperature
 \mathbf{u} bidimensional velocity in the x -direction and y -direction
 W_J Joule energy
 z compressibility factor.

Greek symbols

λ thermal conductivity
 μ viscosity
 μ_0 vacuum magnetic permeability
 ρ density
 σ electrical conductivity.

1. Introduction

Circuit breakers must switch an electrical network as rapidly as possible when a default occurs. Their defective working may have serious consequences. The interruption of an electrical circuit occurs always through the creation of an electrical arc between the electrodes of the circuit breaker. Typically the life time of an electrical arc is 10 ms, half period of current. During this short time very high temperatures exist. It leads to the erosion of the arc contacts and of the circuit breaker walls. The knowledge of the arc behaviour and the prediction of the flow around the arc inside the chamber by numerical simulation is highly useful due to the difficulty to obtain physical quantities with experimental means. Despite the difficulties in having a realistic model of the circuit breaker arc, the numerical approach is then an interesting

* Corresponding author

tool to obtain more precise information on the arc behaviour.

Many works have been published in the literature in the experimental field (Haug et al. [1]; Sponck et al. [2]) or numerical simulation (Gleizes et al. [3]). Authors studied more precisely the interaction of the arc and the gas flow (Ikeda et al. [4]; Trépanier et al. [5]; Thiel and Rutten [6]; Vérité et al. [7]) and the instability of the arc column (Blundell and Fang [8]).

In this work, we have performed a two-dimensional simulation of the arc in a cross-section plane at mid-way between the two electrodes. As a result a particular emphasis was laid on the lateral confinement of the arc and the electrodes effects were neglected. The model is based on the compressible Navier–Stokes and energy equations including electric, magnetic and radiative contributions with real thermodynamic properties. The arc was computed throughout an interruption operation and a particular stress has been put on the effects of the pressure, of the magnetic forces and of the viscosity on the arc behaviour.

2. Configuration, model and numerical treatment

2.1. Configuration

We studied an electrical arc in a model circuit breaking chamber presented in Fig. 1 with the geometrical characteristic dimensions. This breaking chamber is used to obtain experimental values for the electrical arc in low voltage. The arc is initiated by the displacement of a mobile contact which opens the circuit. The electrical arc initially created between the mobile contact and the upper electrode settles quickly between the two electrodes. It is then moved by the electromagnetic forces towards the extinguishing zone of the chamber. We can define characteristic scales for this study: the scale of length is the centimetre, the scale of time is the millisecond and, then, the scale of velocity is 10 m s^{-1} .

Our approach is a two-dimensional simulation in a horizontal plane, perpendicular to the side walls (see Fig. 1). In this plane, the influence of the side walls is privileged and the arc column which is considered as vertical and independent of the vertical coordinate appears through its cross-section. To perform such a simulation of the arc behaviour in the breaking chamber, different assumptions have to be made (Rachard [13]). They are presented hereafter.

2.2. Model

The electrical arc is a plasma, i.e. made up with a mixture of ions, electrons and neutral particles. As a result, the simulated medium differs greatly from a classical room temperature gas. The thermodynamic proper-

ties are strongly variable as a function of temperature and pressure. Such a fluid can be treated as a ‘continuum’ because it is ‘collision dominated’, i.e. the mean free paths for particle collisions are smaller than the characteristic length for macroscopic changes. In our conditions the local thermodynamic equilibrium is valid.

The fluid is described by the compressible Navier–Stokes equations coupled with an energy equation and a state law. The state of the fluid is then characterized by the following thermodynamic variables: the pressure p , the temperature T and the density ρ . The other variables appearing in the equations are: the total energy E and internal energy density e , the speed of sound c , the coefficient of compressibility z , the electrical conductivity σ , the thermal conductivity λ , the dynamical viscosity μ and the velocity \mathbf{u} . The governing equations can then be written as follows:

- *Mass conservation equation*

$$\frac{\partial \rho}{\partial t} + \text{div}(\rho \mathbf{u}) = 0.$$

- *Momentum conservation equation*

$$\frac{\partial \rho \mathbf{u}}{\partial t} + \text{div}(\rho \mathbf{u} \cdot \mathbf{u} + p \mathbf{I}) = \text{div}(\boldsymbol{\tau}) + F$$

where $\boldsymbol{\tau}$ is the stress due to the viscosity forces. $\boldsymbol{\tau} = \mu(p, T)(\text{grad } \mathbf{u} + \text{grad}' \mathbf{u}) - \frac{2}{3}\mu(p, T) \text{div}(\mathbf{u})\mathbf{I}$, and F the Laplace force. \mathbf{I} is the unit matrix.

- *Energy conservation equation*

$$\frac{\partial E}{\partial t} + \text{div}((E+p)\mathbf{u}) = \text{div}(\boldsymbol{\tau}\mathbf{u}) + \text{div}(q) + W_j - R_{\text{ay}}$$

where $q = -\lambda(p, T) \text{grad}(T)$ is the flux of conduction, W_j the Joule energy and R_{ay} the net emission of radiation.

- The state law equation permits the number of equations to match the number of unknowns.

2.3. Joule effect

The electrical arc is a partially ionized gas and has a high capacity of conducting electricity, mainly through the free electrons. For the air, this electrical conductivity σ is zero at the usual temperatures, until 5000 K. From this value it increases significantly. The global resistance of the arc can be written in the form: $R_{\text{arc}} = (h/\int_{S_a} \sigma \text{d}s)$. h and S_a are the geometrical characteristics of the arc column, h its length and S_a its section corresponding to the conducting zone.

Concerning the electrical field E_{arc} in the arc column, we consider that E_{arc} is oriented normally to the simulation plane with a spatially constant intensity only varying with time. The current density flux $j(x, y, t)$ is derived from the knowledge of current $i(t)$, imposed by the power supply installation and the arc section S_a . The Ohm's law

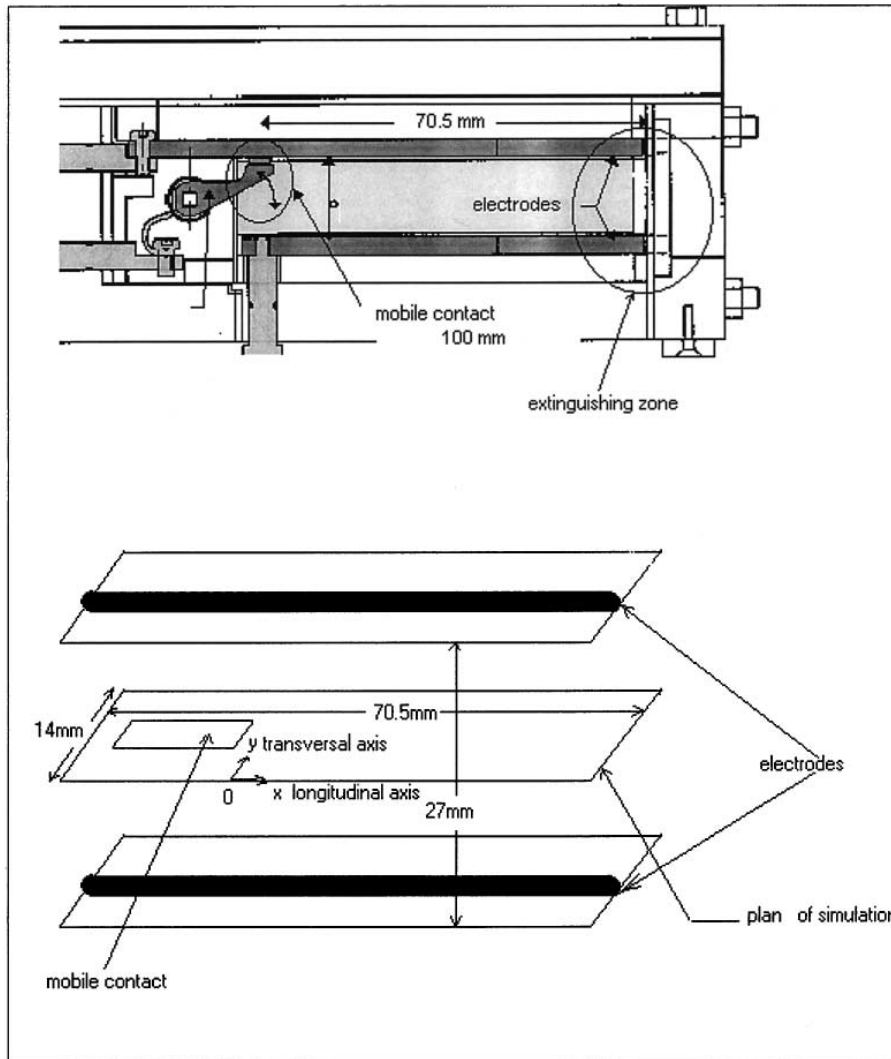


Fig. 1. Model of breaking chamber used for the validations of modelisation. Illustration of the numerical study plane.

gives a relation between the current density j and the electrical field E_{arc} :

$$j(x, y, t) = \sigma(x, y, t)E_{arc}(t)$$

which gives

$$E_{arc}(t) = \frac{i(t)}{\int_{S_a} \sigma ds}$$

The Joule effect which is the electrical energy spent through the arc is then determined by the relation:

$$W_j(x, y, t) = \sigma(x, y, t)E_{arc}^2(t)$$

2.4. Radiation model

The radiation emitted by the plasmas has a spectral distribution which depends on the temperature and the

density. As the radiation is escaping the plasma, emission and absorption phenomena occur along the path. The radiative flux divergence in an elementary volume corresponds to the difference between the radiative power of this volume and the radiation absorbed by the volume: this radiative flux divergence is called net emission. In our model, this quantity is tabulated as a function of the temperature, the pressure and the concentration of metallic vapours coming from the electrodes vaporization [9]. With this net emission term introduced in the energy equation, the radiative transfer is taken into account as net losses in the hot zones. The cold ambient gas is assumed to be transparent, and the possible transfer to the cold zones by absorption of radiation by the lateral walls is not considered.

2.5. Thermodynamical model and state law

In the composition of dry air plasmas, we can note the presence of concentration peaks of various species. The plasma composition is function of the gas temperature, its variations corresponding to molecules dissociation. As a consequence, the thermodynamical properties change strongly with temperature and pressure. By a theoretical approach, Cheminat [10] has calculated these properties, namely, the dynamical viscosity $\mu(p, T)$, the thermal conductivity $\lambda(p, T)$, the electrical conductivity $\sigma(p, T)$ and the compressibility factor $z(p, T)$.

$z(p, T) = (p/\rho r_0 T)$ is introduced in the usual perfect gas equation as a multiplicative factor to take into account the variations of the plasma composition.

2.6. Magnetic induction and Laplace force

The magnetic induction in the circuit breaker is created either by the conductive elements present in the breaker (electrodes and metallic parts) or by the arc itself. The first contribution constitutes an outer field which will move the arc globally (see Fig. 2). The second contribution will rather act on the static structure of the arc. The attraction between the current lines induces a contraction of the arc column which prevents the arc spreading. This phenomenon is called 'striction'. The influence from both magnetic field sources is considered in our model. To determine the magnetic induction due

to the electrodes, we use the Biot–Savart's law giving the induction created at a point M by a linear conductor :

$$B(M) = \frac{\mu_0 i}{4\pi} \int_l \frac{dl \wedge r}{r^3} \quad (1)$$

where dl represents an element of the conductor and r is the vector joining the element and M . For a point M in the plane at mid-height between the two electrodes, the magnetic induction takes the value $\mu_0 i/4\pi h$. In fact, as the induction grows strongly near the electrodes, this value is underestimated and would not account for the real induction acting on the whole arc column. It is better to consider a mean magnetic induction, $\bar{B} = (\mu_0 i/4\pi) \int_{h_0}^h [(dz/(h-z))]$, where h_0 , close to h , is the length of integration, or $\bar{B} = (\mu_0 i/2\pi h)\bar{K}$, where \bar{K} is a constant depending on h_0 . Practically, different values of \bar{K} have been used, between $\bar{K} = 5.4$ and $\bar{K} = 20$. We have also taken into account the fact that the arc has a thickness along x . The current in the electrodes decreases from the complete value at the level of the arc tail to small values at the level of the arc head which corresponds to the last current lines.

Concerning the induction due to the arc itself (self induction), we assume that the arc is built up by elementary filaments with known current density. The self induction at a point M of the arc section is the sum of the contributions of the different filaments issued from the points K of the arc section : $B_{S_a}(M) = \sum_{K \in S_a, K \neq M} B_K(M)$.

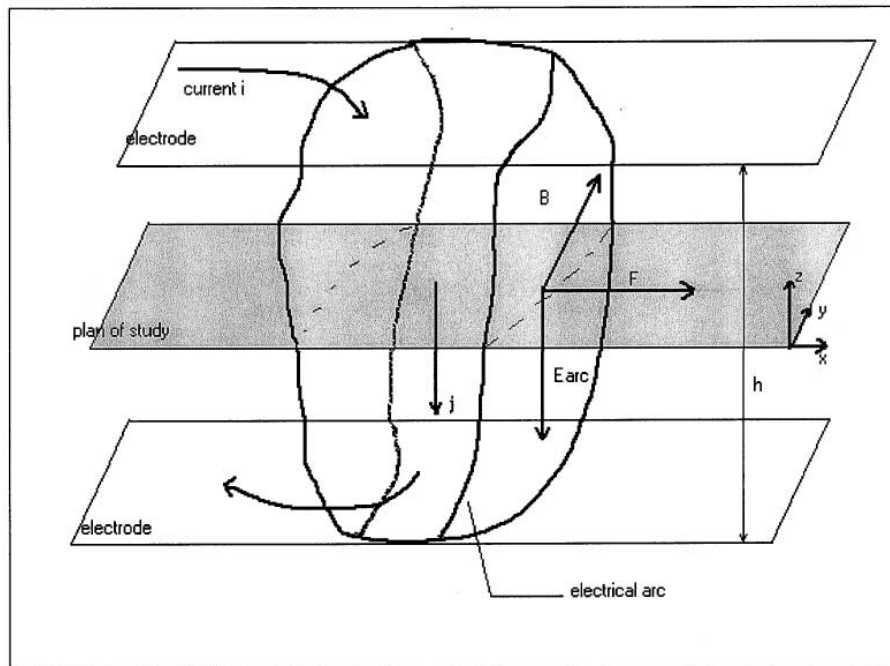


Fig. 2. Direction of principal electromagnetic field. The self magnetic induction and the resulting forces ("striction") are not represented.

Each contribution $B_k(M)$ is evaluated by the Biot–Savart's law [equation (1)].

The Laplace force is $F = j \wedge B$, where B is the total magnetic induction, sum of the inductions created by the electrodes and by the arc itself.

2.7. Numerical method

The resolution of the problem, characterized by high speed compressible flows with sharply varying gradients between the very hot electrically conducting zones and the cold zones, needs a specific numerical method. We use a method which was initially developed for transonic and supersonic flows [11]. This method uses a finite element approximation for the diffusive terms and a finite volume approximation for the convective terms. As in most numerical methods used in compressible flows, the treatment of these convective terms is based on the characteristic directions of propagating waves. Also one of the problems is to approximate with precision the sound velocity for high temperature thermodynamic states for which the perfect gas state law does not apply. The method implemented in the code is based on the one developed by Glaister [12] for the non viscous flows (Euler equations) of real gases with a state law of the form $p = f(\rho, e)$. Adjustments have been necessary hence in our problem, the state law is not known explicitly, but through the tabulated values of the compressibility factor $z(p, T)$ [13].

The numerical scheme is explicit in time with a time step Δt limited by a CFL stability condition. The discretization is of second order in time and it is of first order in space.

The imposed boundary conditions are based on the study of hyperbolic systems with the methods of characteristics. The boundary conditions depend on the type of boundaries and on the nature of the flow. In our problem, these conditions are simple as we are concerned by solid boundaries and subsonic flows. We use no-slip conditions with wall temperature forced to 300 K.

3. Characteristic evolution of the electrical arc in a closed chamber

Before studying the influence of different contributions on the arc behaviour, we first present a characteristic evolution of the electrical arc in the breaking chamber.

3.1. Parameters of the simulation

The chamber is considered as completely closed with impervious rigid walls. These walls are maintained at a fixed temperature of 300 K; this condition, although approximate, is better than an adiabatic condition because it allows loss of energy at the walls. In the cal-

culaton, the arc is initiated through a local injection of energy just ahead of the mobile contact. This energy corresponds to a power density of $2 \times 10^{11} \text{ W m}^{-3}$. When the temperature is locally 10 000 K, which corresponds to a time of 27.5 μs , the forced heating is stopped but as the fluid is now conductive, the current is then imposed. The Joule effect becomes effective and the arc can then develop. The peak of the sinusoidal current is 2410 A, its frequency is 60 Hz. The lifetime of the electrical arc is on 7 ms. Experimentally, in the same conditions the arc crosses the model cavity in 2 ms.

3.2. Characteristic evolution

This initialization represents a wire fuse ignition of an arc. The arc apparition corresponds to a very quick and intense heating, as an explosive phenomenon. A pressure wave is then generated which moves across the cavity with a diminishing intensity. The arc changes quickly from its initial circular shape to an ellipsoidal shape, essentially due to the lateral walls confinement. The arc temperature grows sharply during the first 100 μs , reaching a maximal level of 17 500 K before decreasing slowly until stabilization at a mean level of 15 000 K around $t = 500 \mu\text{s}$ (Fig. 3).

In the case presented here, the arc does not move much inside the cavity but rather spreads to fill the whole width of the cavity. The magnetic force due to the electrodes seems to be not sufficient to push the arc; it is the thermal expansion limited by the magnetic striction which appears to be predominant. During the first part of the evolution until 400 μs , the pressure waves play a major role. They travel through the length of the cavity within a time of 100 μs . They are visible on the pressure fields (Fig. 4), but also on the velocity vector fields as they strongly influence the flow in the breaking chamber through the associated speed wave. For example at $t = 200 \mu\text{s}$, the main pressure wave initiated on the right of the arc has been reflected on the rightmost wall and travelling then towards the left it interacts with the arc. This pressure wave is clearly visible in Fig. 5 on the velocity field, as it forces the velocities towards the left. It influences also directly the behaviour of the arc, which happens to be compressed and to recede slightly as the wave passes. After $t = 400 \mu\text{s}$, the pressure wave is strongly attenuated and it does not perturb significantly the further evolution of the arc. The typical structure of the flow around the arc can then be observed (Fig. 6).

In the hot arc core the velocities are created towards the right whereas colder fluid is carried reversely along the lateral walls from the front of the arc to its back. The resulting velocity field in the plasma consists in two symmetrical vortices on each side of the longitudinal symmetry axis of the cavity (Fig. 6). These vortices have been already mentioned, for instance by Jones and Fang [14]. These plasma velocities which result from the mag-

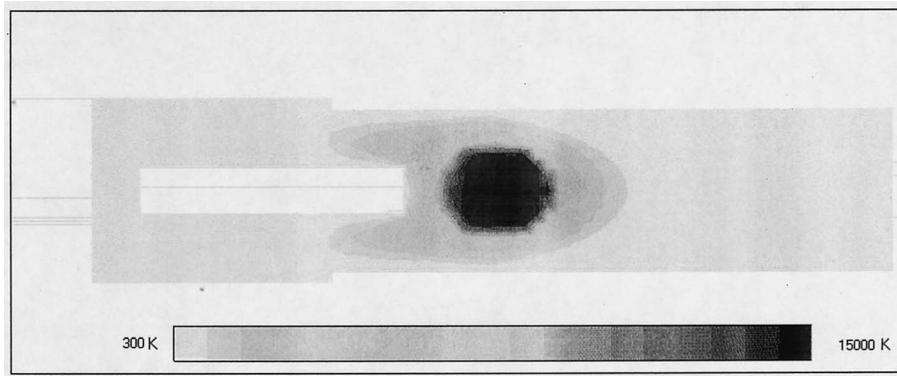


Fig. 3. Isotherms at $t = 500 \mu\text{s}$. Characteristic shape of the arc.

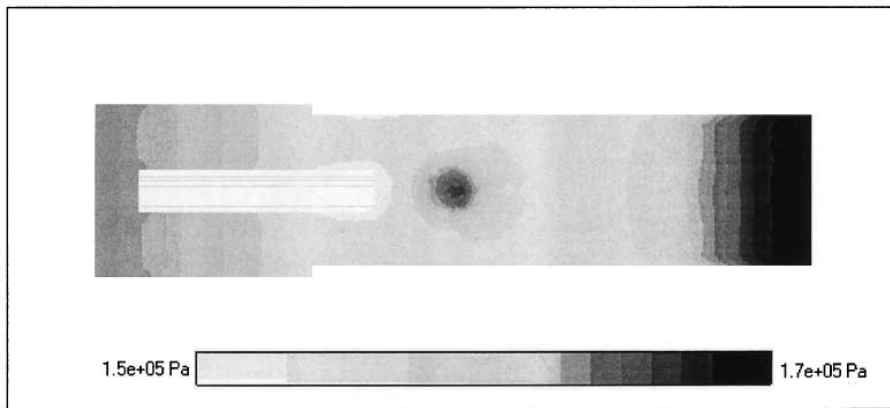


Fig. 4. Isovalues of pressure at $t = 300 \mu\text{s}$. Note the presence of pressure waves due to the extremely rapid arc ignition and of an overpressure (300 mb) in the arc column.

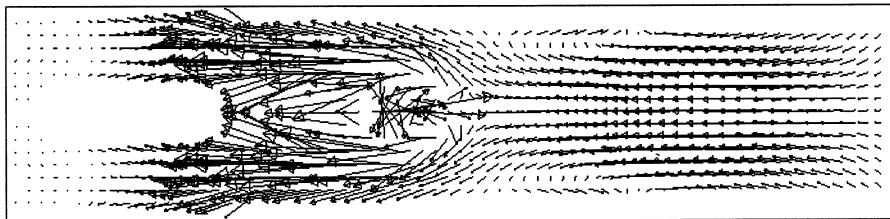


Fig. 5. Velocity vector field at $t = 200 \mu\text{s}$. Note the strong backflow due to a left moving pressure wave.

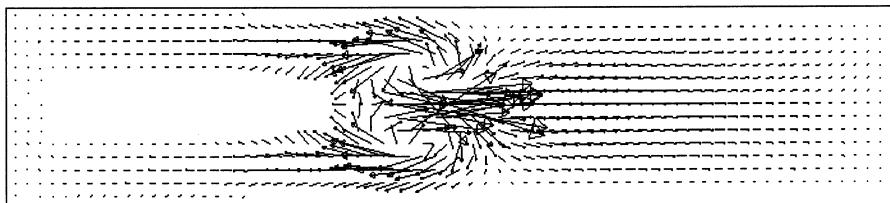


Fig. 6. Velocity vector field at $t = 500 \mu\text{s}$. Note the presence of the characteristic symmetric two vortices flow.

netic force counterbalanced by the pressure gradients and the inertia and viscous forces are about 100 m s^{-1} , but the arc displacement velocity is much weaker (10 m s^{-1}). This difference can be explained by the very weak density of the hot plasma. The strong velocities in the arc core affect few particles which are not able to push away the more dense external gas. As a result of the weak density, the arc seems to behave like a rigid medium. In our study the arc is similar to a moving piston, which results in a difference of pressure between the front and the back of the arc. A systematic overpressure is also observed in the hot arc zone.

The variation of the electrical quantities can be observed during the lifetime of the arc. The time evolution of the arc resistance is presented in Fig. 7. This resistance varies as the inverse of $\int_{s_1}^{s_2} \sigma ds$ and depends strongly on the temperature and size of the arc. It decreases sharply during the first $100 \mu\text{s}$, i.e. during the time when the size and the temperature of the arc increase strongly. At about $200 \mu\text{s}$ the resistance presents a peak corresponding to the contraction of the arc as the pressure wave passes (the other interactions of the pressure waves with the arc are not so well visible). The arc resistance decreases then more slowly as the characteristics of the arc (temperature and size) become more steady. The voltage and the electric field (characteristic values, respectively: 80 V , 3000 V m^{-1}) which depend on

the arc resistance through the Ohm's law present similar evolutions.

Some precisions on the dynamical equilibrium inside the cavity can be obtained through dimensionless numbers related to the momentum equation. These numbers are evaluated from the characteristic velocity U of the hot plasma (about 100 m s^{-1}), the characteristic length D which is the transversal length of the breaking chamber, and thermodynamical properties:

- The magnetic pressure number $S = (B^2/\mu_0\rho U^2)$ which corresponds to the ratio of the two dominant terms determining the arc motion, the magnetic force F and the pressure force $\text{div}(pI)$ [S can be noted as $S = (1/Al^2)$ where Al is the Alfven number used in astrophysics]. The pressure term is about 5.10^6 N m^{-3} and depending on the constant K , the magnetic term may vary between 10^7 and $5 \times 10^7 \text{ N m}^{-3}$, which gives for S a value about several unities. The two forces balance each other.
- The usual Reynolds number: $Re = (\rho UD/\mu)$. Its value is weak in the hot zone ($Re \approx 10$) and stronger outside ($Re \approx 10000$), which indicates that the occurrence of turbulence would be only possible outside the arc zone.
- At last the weak value of the magnetic Reynolds number: $Re_m = P_r Re \approx 0.02$ ($P_r = \mu_0(\mu/\rho)$ is the magnetic Prandtl number) indicates that the induced mag-

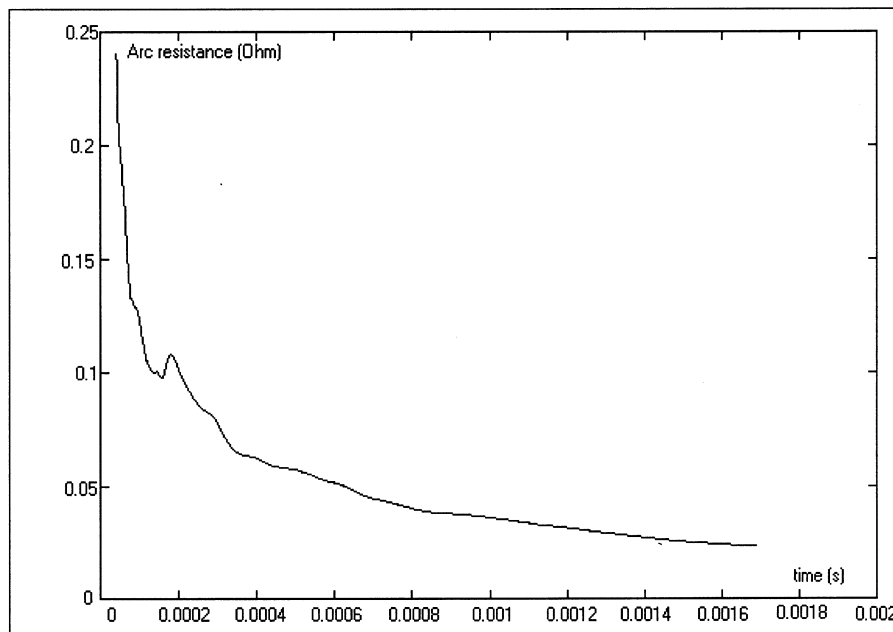


Fig. 7. Variation with time of the arc resistance—3 phases may be noted. During the first $100 \mu\text{s}$, the arc resistance decreases sharply, the arc is growing. At $t = 200 \mu\text{s}$, a little peak shows the arc compression by a pressure wave. Beyond $t = 400 \mu\text{s}$, the arc resistance decreases slowly, which means that the arc size and temperature are more steady. The corresponding voltage in the arc decreases from 180 to 50 V.

netic field (connected to perturbations by the fluid motions) can be neglected to the outside imposed magnetic field.

4. Influence of the magnetic force on the arc behaviour

4.1. Electrodes magnetic force: dynamic and stagnant cases

In the breaking chamber the flow and arc dynamics are considerably changed when the intensity of the electrodes magnetic Laplace force is modified. In the previous section, a rather stagnant arc was presented. Increasing the magnetic force leads to more dynamic cases. One of them which is closer to the experimental observations and for which the arc moves to the right endwall within a time of around 1.5 ms is presented hereafter.

In Fig. 8 is given the time evolution of the temperature field, it may be noted that the arc is generally smaller and slightly colder than in the stagnant case. In fact, the arc moves more easily and the cooling by the exchanges with the surrounding gas is improved. However the balance between the different thermal contributions (principally the Joule heating and the radiation losses) still gives a mean temperature close to 15 000 K. Around $t = 1$ ms, an increase of the temperature is observed which is connected to stronger current densities due to the decrease of the arc section. Some hot areas with a mean temperature around 6000 K also persist behind the arc within the domain that was crossed over by the arc. In these zones a new arc may appear which could lead to the failure of the breakdown.

The pressure levels are also stronger than in the stagnant case. The piston effect created by the arc displacement is responsible for the strong pressures observed ahead of the arc in the closed chamber. Behind the arc the pressure decreases regularly until the left endwall (Fig. 9).

The action of the force due to the electrodes magnetic field should induce a continuous acceleration of the arc (moreover this force increases as the square of the increasing current). In fact this acceleration is mainly effective during the first part of its displacement corresponding to a time of 800 μs . Afterwards the arc speed rather decreases because of the increasingly compressed gas ahead of it. The mean arc speed is around 30 m s^{-1} which still is a small value compared to the velocities in the hot plasma which vary between 50 and 300 m s^{-1} . After the attenuation of the pressure waves, the typical two-vortex velocity structure is obtained. This structure seems globally transported during the displacement of the arc. Behind the arc in the whole domain at 6000 K a quite uniform backward velocity field is observed, kind of drag flow induced by the moving arc.

At last, when the arc gets close to the right endwall

(beyond $t = 1.5$ ms), the arc temperature field is less homogeneous (Fig. 8) and the velocity field is strongly non uniform.

4.2. Striction force

In order to obtain more information on the role of the striction force, the stagnant case has been recomputed without this force. In this new case, as can be seen in Fig. 10, the arc has not a global homogeneous displacement but rather spreads out in the direction of the electrodes magnetic force. At $t = 3$ ms, the arc front has progressed towards the right endwall while the arc tail is still near the mobile contact. The arc has then lost its concentrated circular shape. These indications show that the striction force allows the arc to keep its coherence but also restrains its displacement.

The two-vortex velocity structure (Fig. 11) persists without striction force but the structure is stretched and occupy the whole arc zone. During the arc evolution, as shown in Fig. 12, the pressure field is quasi mono-dimensional, uniform behind the arc, linearly increasing within the arc domain, and still uniform at a higher pressure level ahead of the arc. The overpressure observed previously in the arc zone is not obtained, which indicates that it comes from the striction force and it creates an effect opposed to the latter. The thermal expansion is also a phenomenon opposed to the striction force. It corresponds to motion of fluid particles outwards of the zones with increasing temperature and towards the zones with decreasing temperature. A computation performed without any magnetic force has shown that the velocities created by thermal expansion can be important, up to 100 m s^{-1} , during the first 100 μs when the temperature of the arc increases strongly and that they can lead to a quicker expansion of the arc compared to what is obtained only by diffusion. Later these velocities diminish and become rather small after 500 μs when the temperature in the arc is stabilized. In a real case (with magnetic forces) the strong thermal expansion during the initial arc temperature increase is in direct competition with the strong striction forces which tend to squeeze the arc column.

4.3. Summary

The typical two-vortex velocity structure is due to the electrodes magnetic force. This force pushes the hot plasma zones towards the right endwall. The stronger it is, the quicker the arc displacement. Because of this displacement, this force is also responsible for overpressures localized ahead of the electrical arc which acts like a piston.

The striction force allows the arc to remain compact and induces overpressure in the arc zone. This force is also in competition with the thermal expansion which

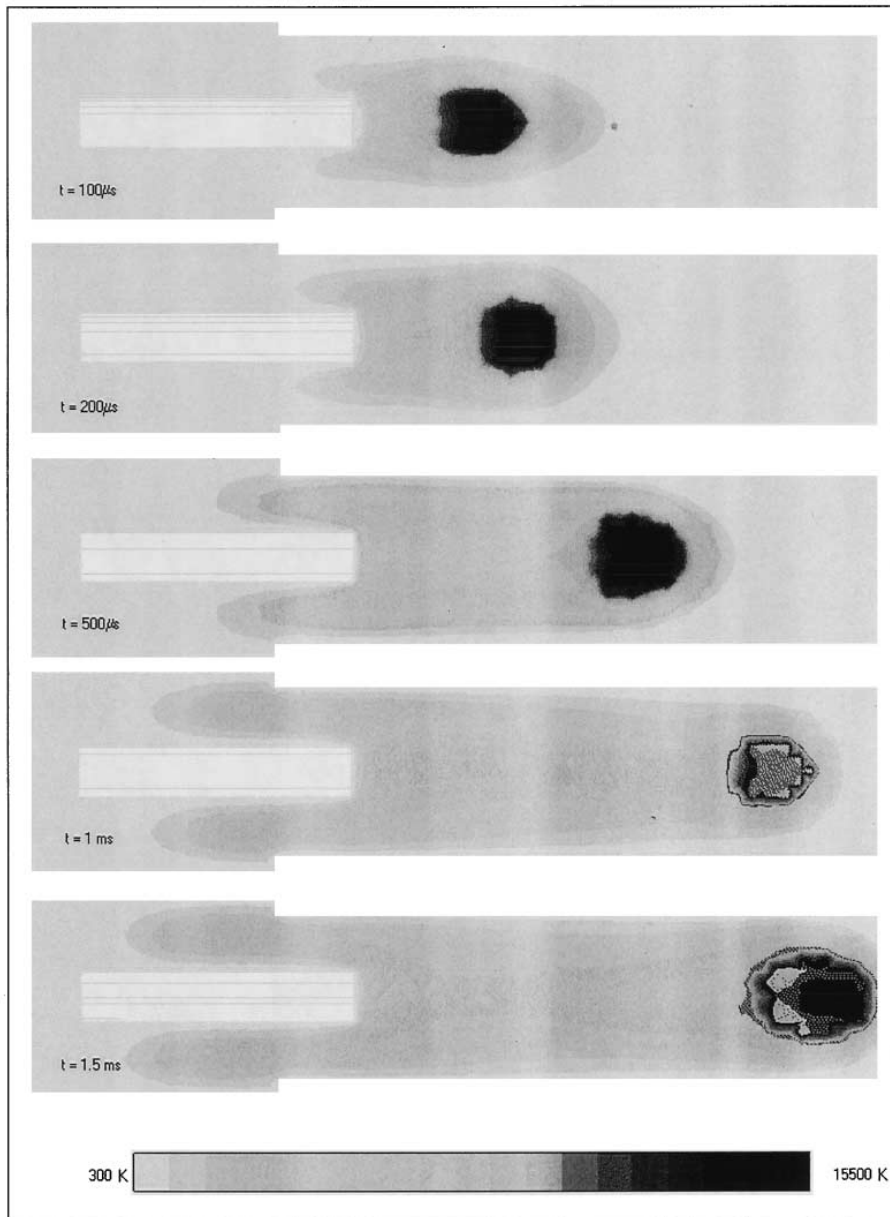


Fig. 8. Dynamic case. Evolution of the arc given through temperature fields taken at different times. The arc velocity increases during the first 800 μs and then decreases due to the presence of the chamber end. Its temperature is generally about 15000 K and then decreases to 12500 K beyond $t = 2 \text{ ms}$. The arc drag is at about 6000 K.

is a relatively important phenomenon during the initial temperature increase.

The magnetic forces do not really influence the mean temperature in the arc which is principally determined by the balance between the Joule effect and the losses by radiation.

5. Influence of the viscosity

This influence has been studied in the dynamic case by comparing the results with a specific simulation where the viscosity and the walls adherence have not been taken into account.



Fig. 9. Dynamic case. Pressure field at $t = 400 \mu\text{s}$. Overpressure in the arc column and ahead of the arc. The pressure increases globally with time in the chamber.

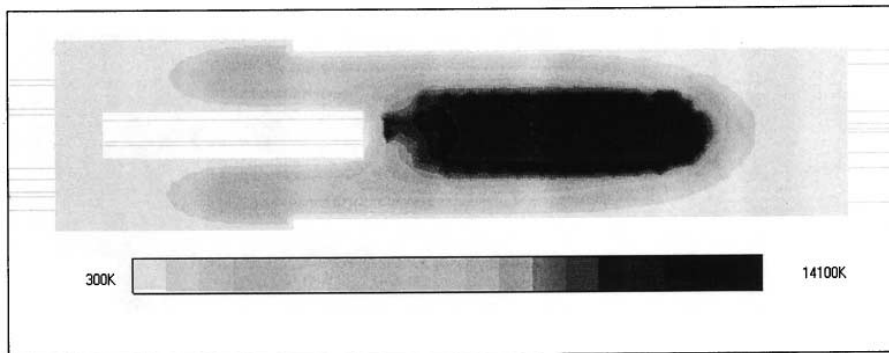


Fig. 10. Case without striction force. Isotherms at $t = 3 \text{ ms}$. Spreading of the arc.

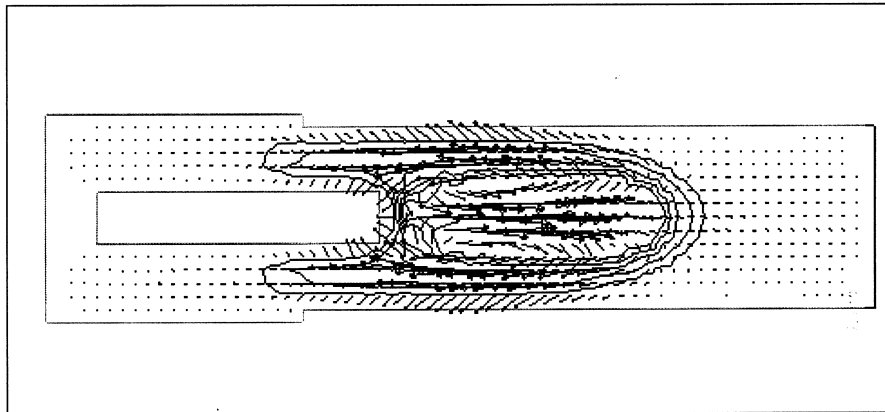


Fig. 11. Case without striction force. Velocity field and isotherms at $t = 1.5 \text{ ms}$. The characteristic two-vortex velocity structure is stretched. At the arc boundaries, the velocities show the thermal expansion.

A comparison between the two evolutions shows that the results are very similar (temperature level, size of the arc, velocity intensities...). Some differences can be observed on the pressure levels and on the velocities. As it can be seen on the longitudinal profiles of pressure in Fig. 13, the pressure levels are weaker without viscosity. Concerning the velocity, the absence of viscous stresses

allows the arc to move slightly more quickly, the arc reaching the right-endwall within 1.2 ms compared to 1.5 ms if viscosity is taken into account. The flow moving back along the walls on each side of the arc is easier in the absence of viscosity (see Fig. 14 for $t = 100 \mu\text{s}$). This backflow limits slightly the lateral expansion of the arc. At last, the transverse velocity profiles obtained in the

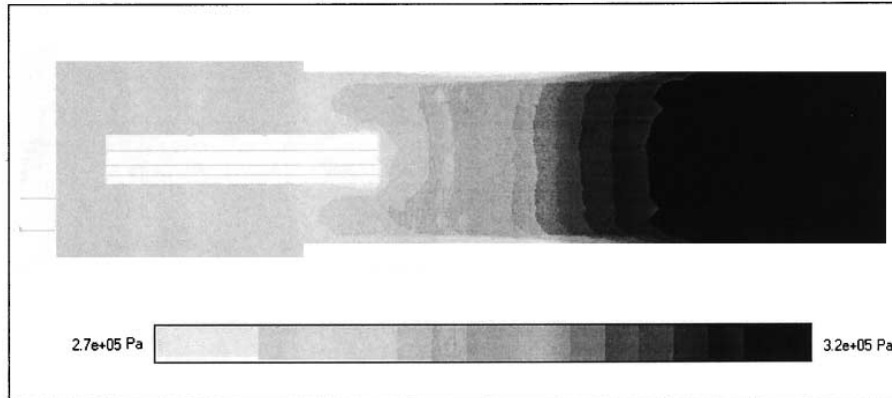


Fig. 12. Case without striction force. Isovalues of pressure at $t = 3$ ms. Warm gases are compressed in the right part of the chamber due to the arc displacement (piston effect). The overpressure in the arc column has disappeared.

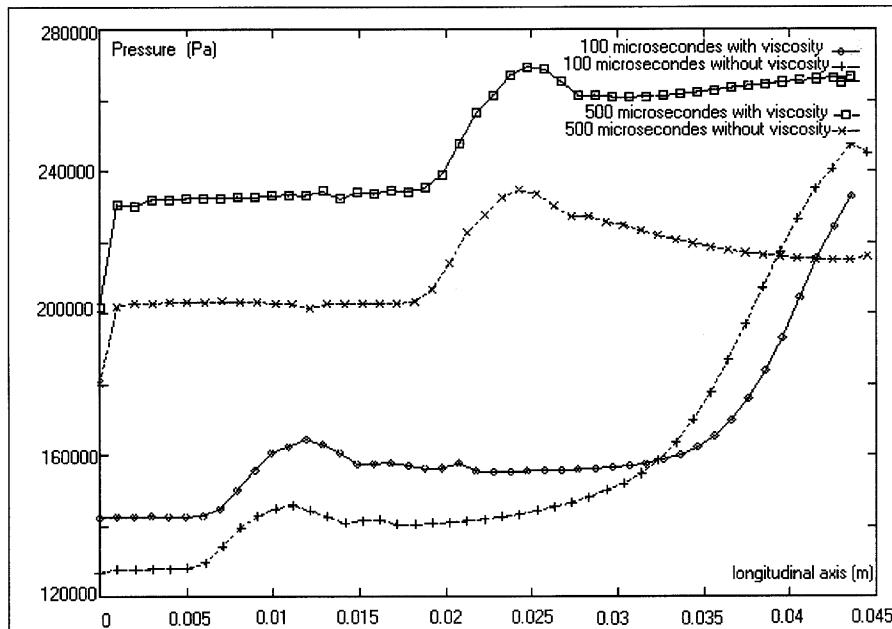


Fig. 13. Comparison between two cases, with and without viscosity. Longitudinal pressure profiles at $t = 100 \mu\text{s}$ and $t = 500 \mu\text{s}$. The bumps on the profiles correspond to the overpressure in the arc zone.

drag flow behind the arc (see Fig. 14 for $t = 500 \mu\text{s}$) show that the two near-wall back flows are still present without viscosity whereas they have joined to give an almost parabolic drag flow in the viscous case.

6. Conclusion

We used a numerical compressible code to simulate the physical phenomena occurring during a current interruption operation. It seems that the fluid compressibility coupled with a judicious treatment of state law is an

important feature for the simulation of very hot gases flows as plasmas in cold gases.

The arc has been simulated during a few milliseconds. We have shown at the beginning of the simulation that the pressure waves generated by the extremely rapid arc ignition have a strong influence on the arc shape and its displacement. Later, overpressures are found in the arc zone due to the magnetic striction force and ahead of the arc due to the arc displacement induced by the electrodes magnetic force. The temperature level and the size of the arc first increase rapidly, and then stabilize when the temperature approaches a value of 15 000 K as a conse-

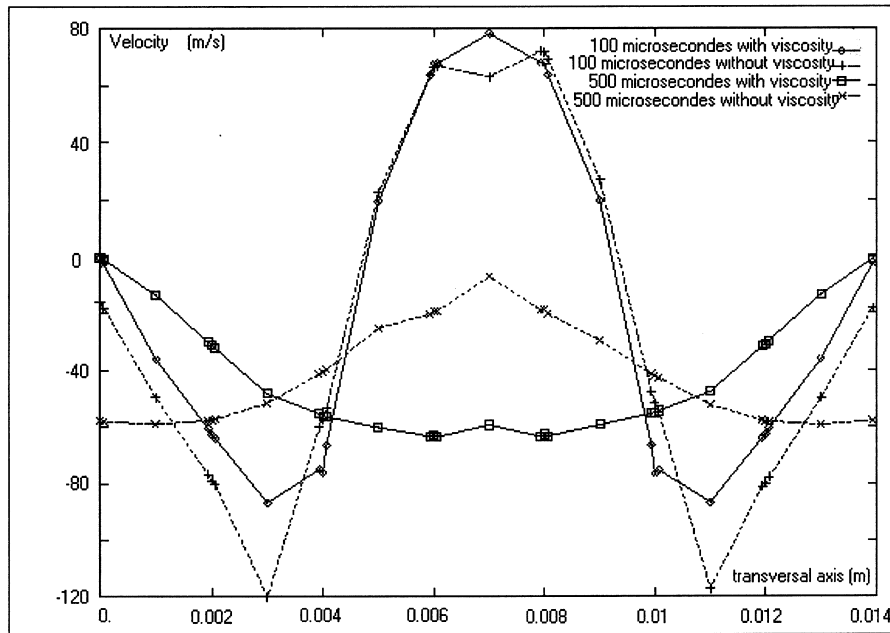


Fig. 14. Comparison between two cases, with and without viscosity. Longitudinal pressure profiles at $t = 100 \mu\text{s}$ and $t = 500 \mu\text{s}$. The bumps on the profiles correspond to the overpressure in the arc zone.

quence of the balance which prevails between Joule energy production and radiation losses. Depending on the electrodes magnetic field intensity, the arc can be stagnant or very rapid (the displacement velocity can be up to 30 m s^{-1}). The velocities are still more intense in the plasma and the flow appears in the form of typical two vortices. The striction forces maintain the coherence of the arc which otherwise would spread under the influence of the thermal expansion and of the electrodes magnetic forces. During the arc displacement, a drag flow is observed behind the arc with a temperature around 6000 K . As regards the viscosity, it seems that it has not an important influence on the results mentioned.

References

- [1] Haug R, Hahn R, Benabdelhamid F. Planimètre électromagnétique pour circuits électriques—diagnostic d'un arc électrique. *Meas Sci Technol* 1990;1.
- [2] Sponck L, Scarpa P, Legros W, Fiévet C. Investigation on heat fluxes in a circuit breaker. XIIth Symposium on Physics of Switching Arc. Brno, October 1996.
- [3] Gleizes A, Gonzalez JJ, Razafinimanana M. Arc-anode interaction. XIIth Symposium on Physics of Switching Arc. Brno, October 1996.
- [4] Ikeda H, Suzuki K, Okamoto M, Ohaski H, Kobayashi A. Analysis of gas flow associated with SF6 gas circuit breaker. 10th Int Conf on Gas Discharges and Their Applications. Swansea, 1992, pp. 90–5.
- [5] Trepanier JY, Reggio M, Camarero R. LTE computational of axisymmetric flow interaction in circuit breakers. *IEEE Transactions on Plasma Science* 1991;19(4):580–9.
- [6] Thiel HG, Rutten U. Modelling of a high current arc as energy source in computational fluid dynamics. 10th Int Conf on Gas Discharges and Their Applications. Swansea, 1992, pp. 932–5.
- [7] Vérité JC, Boucher T, Comte A, Delalandre C, Robin-Jouan Ph, Serres E, Texier V, Barrault M, Chévrier P, Fiévet C. *IEE Proc Sci Meas Technol* 1995;142(3).
- [8] Blundell RE, Fang MTC. Stability of an axially uniform arc in accelerating flow. XIIth Symposium on Physics of Switching Arc. Vol. 1, Brno, October 1996.
- [9] Rahmani B. Calcul de l'émission nette du rayonnement des arcs dans l'hexafluorure de soufre (SF6) et dans les mélanges SF6-Azote. Thèse Université Paul Sabatier, Toulouse III, 1989.
- [10] Cheminat B. Communication privée, 1987.
- [11] LeRibault C. Simulation des écoulements turbulents compressibles par une méthode mixte éléments finis-volumes finis. Thèse Ecole Centrale de Lyon, 1991.
- [12] Glaister P. An approximate linearized solver for the Euler equations for real gases. *Journal of Computational Physics* 1989;74:382–408.
- [13] Rachard H. Etude par simulation numérique des phénomènes couplés électromagnétiques et aérodynamiques au sein d'un arc de coupure. Thèse Ecole Centrale de Lyon, 1995.
- [14] Jones GR, Fang MTC. The physics of high power arcs. *Rep Prog Phys* 1980;43.